Communication

Electrochemiluminescence Self-Interference Spectroscopy with Vertical Nanoscale Resolution

Yafeng Wang, Weiliang Guo, Qian Yang, and Bin Su

J. Am. Chem. Soc., **Just Accepted Manuscript** • DOI: 10.1021/jacs.9b12833 • Publication Date (Web): 08 Jan 2020

Electrochemiluminescence Self-Interference Spectroscopy with Vertical Nanoscale Resolution

Yafeng Wang, Weiliang Guo, Qian Yang and Bin Su*

Institute of Analytical Chemistry, Department of Chemistry, Zhejiang University, Hangzhou 310058, China

Supporting Information Placeholder

ABSTRACT: Here we report an electrochemiluminescence (ECL) self-interference spectroscopy technique (designated as ECLIS) with spatial resolution in the normal direction of electrode surface. Self-interference principally originates from the superposition of ECL emitted directly by luminophores and that reflected from electrode surfaces, resulting in a spectrum consisting of orderly distributed peaks. Based on this spectrum and theoretical analysis by matrix propagation model, the distance between luminophores and electrode surface can be probed with a vertical resolution in the nanometer scale. We demonstrated firstly in this work that the height of ECL luminophores assembled on the electrode surface using different molecular linkers, such as double stranded DNA, could be determined, as well as possible conformation of linker molecules at the surface. Moreover, the thickness of ECL emitting layer adjacent to the electrode surface was estimated for the classical coreactant ECL systems involving freely diffusing $Ru(bpy)_3^{2+}$ and tri-*n*-propylamine in solutions. The thickness was found to vary from ~350 nm to near 1 μm, depending on the concentration of $Ru(bpy)_3^{2+}$. We believe that ECLIS with a high vertical resolution will provide an easy way to collect molecular conformation information and study ECL reaction mechanisms at electrode interfaces.

Electrochemiluminescence (ECL) is luminescence in which the emissive excited state is generated by electrochemical reactions.[1,2] Since the reactions are confined to the surface/vicinity of the electrode and highly sensitive to the surface reactivity, ECL possesses excellent spatially-controlled resolution. For examples, direct ECL imaging of the electrode surface can reveal spatial distribution of active sites. ECL imaging have also manifested itself as a powerful tool for the detection in microelectrochemical and microfluidic systems, visualization of latent fingermarks,[3,4] recognition of metabolite-generated toxicity and multiple biomarkers.[5,6] More recently, ECL microscopy has been developed for imaging cells[7-9] and nanoparticles,[10-13] with the lateral resolution down to nanometers.[14,15] However, only a few works have paid attention to the spatial resolution in the vertical direction of electrode surface. Vertically resolved information is very important for deciphering reaction mechanisms and developing ECL-based immunoassays. For the classical coreactant ECL system of $Ru(bpy)_3^{2+}$/tri-*n*-propylamine (TPrA), the thickness of light emitting layer at the electrode surface is resolved to vary from several hundred nanometers to few micrometers, depending on the coreactant used and the concentration of $Ru(bpy)_3^{2+}$.[16,17] While in microbead-based immunoassays, the vertical distribution of coreactant radicals over a layer comparable to the bead size determines essentially the sensitivity.[18]

Herein we report a novel ECL technique with vertical nanoscale resolution based on the principle of optical interference. Optical interference refers to the superposition of two or more coherent light waves to generate constructive and destructive fringes. For the widely studied thin-film optical interference, light reflected by the film mutually interferes to form orderly distributed peaks in the interferometric spectrum.[19] Optical interference has found wide applications in diverse fields, such as biosensing,[20-22] electrochemistry[23-26] and molecular analysis.[27-29] In this work an ECL self-interference spectroscopy (ECLIS) technique based on interference of ECL in-situ generated at the electrode surface is reported. It was firstly employed to determine the height of luminophores at the electrode surface with vertical nanoscale resolution. It was then applied in measuring the thickness of emitting layer of classical coreactant ECL systems involving freely diffusing $Ru(bpy)_3^{2+}$ and TPrA.

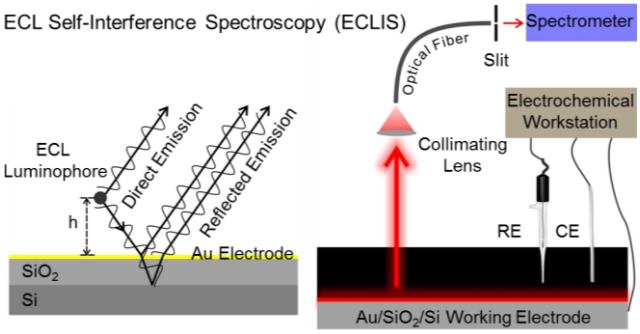

Figure 1. ECL self-interference at the gold/silica/silicon ($Au/SiO_2/Si$) electrode surface (left) and experimental ECLIS measurement (right).

Figure 1 illustrates the principle of ECL self-interference and experimental system for ECLIS measurement (see details in supporting information (SI), Section S1). Under dark conditions, self-interference light originated from the superposition of ECL emitted directly by luminophores (termed as direct emission) and that reflected (termed as reflected emission) by electrode surface is focused by a collimating lens into an optical fiber and finally transmitted to the spectrophotometer after passing through a 200-μm-wide slit. A homemade three-electrode electrochemical cell was used (**Figure S1**), in which the $Au/SiO_2/Si$ electrode acted as the working electrode. This electrode was prepared by electron-beam evaporation of an ultrathin layer of gold onto the SiO_2/Si wafer using titanium as the adhesion. The intermediate SiO_2 layer, with a thickness of ~6.21 μm (**Figure 2a**), plays the crucial role for optical interference. As shown in **Figure 2b**, the evaporation of gold and titanium formed an ultrathin and uniform coating layer. The thickness of gold layer is 11.80 nm (determined by ellipsometry). The gold surface is very smooth with a sub-nanometer roughness (**Figure S2**).

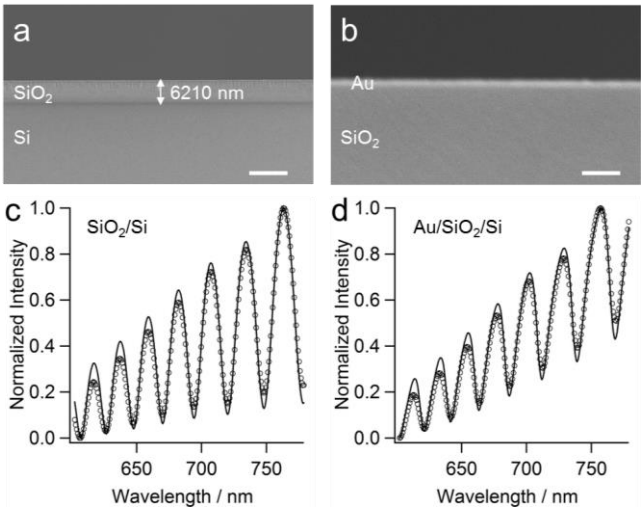

Figure 2. (a, b) Cross-sectional SEM images of SiO_2/Si substrate (a) and Au/SiO_2/Si electrode (b). (c, d) Experimental (open circles) and simulated (solid curves) white light interferometric spectra in air. The scale bars in (a) and (b) are 10 μm and 100 nm.

White light interference in air was firstly studied at the SiO_2/Si substrate and Au/SiO_2/Si electrode using an external light source. The spectra display distinct and sharp peaks in the range from 600 nm to 780 nm (open circles, **Figure 2c** and **d**). The peaks exhibited at the former surface are apparently larger than that at the latter one, due to the reflectivity difference between gold and SiO_2 surfaces. Given the gold surface has a higher reflectance, the light reflected from there is stronger than that at the SiO_2/Si interface (SI, Section S2.1 and **eq. S9**). It means that the gold layer should be as thin as possible.

The interference response can be rationalized by the matrix propagation model (SI, Section S2.2 and **Figures S3-S4**), which simplifies the multilayer film electrode as a single front surface.[19] For the Au/SiO_2/Si electrode consisting of three layers and light incidence at the normal direction, the characteristic matrix is,

$$\begin{bmatrix} B \\ C \end{bmatrix} = \left\{ \prod_{r=1}^{3} \begin{bmatrix} \cos\delta_r & (i\sin\delta_r)/n_r \\ i n_r \sin\delta_r & \cos\delta_r \end{bmatrix} \right\} \begin{bmatrix} 1 \\ n_S \end{bmatrix} \quad (1)$$

where B and C are the normalized electric and magnetic fields at the front interface, respectively. $\delta_r = 2\pi n_r L_r/\lambda$, with n_r and L_r denoting the refractive index and thickness of the r layer. λ is the wavelength. n_s is the refractive index of the substrate. This model essentially offers an easy way to calculate the light reflectance at the front interface,

$$R = \left(\frac{n_0 B - C}{n_0 B + C}\right)\left(\frac{n_0 B - C}{n_0 B + C}\right)^* \quad (2)$$

where n_0 is the refractive index of incident medium. The white light interferometric spectrum can be thus calculated as the product of the intensity of incident light and the reflectance (R, **eq. 2**) at different wavelengths (SI, Section S2.3 and **Figures S5-S6**). As shown in **Figure 2c** and **d**, the calculated spectra (solid curves) match well with experimental ones. Taking a minimum of least-squares deviation between two spectra as the criterion, the thickness of SiO_2 layer was estimated to be 6.44 μm, close to that determined from SEM image.

Instead of using external light, ECL in-situ generated at the electrode surface can function as the source to generate interference. We firstly examined the vertical resolution of ECLIS with monolayer films of luminophores. 3-Mercaptopropionic acid (MPA) and double stranded DNA (dsDNA) consisting of fifty base pairs (50-bp) were used as short and long linkers, respectively, the distal ends of which bear $Ru(bpy)_3^{2+}$-derivatized luminophores (**Figure 3a** and **c**). **Figure 3b** and **d** display the ECLI spectra using 2-(dibutylamino)ethanol (DBAE) as the coreactant. In both cases, distinct and orderly distributed spectral peaks are observed in the range from 550 nm to 850 nm, confirming the occurrence of ECL self-interference. By contrast, if a gold coated glass (Au/glass) electrode was used, only normal ECL spectra with a single peak were obtained (**Figures S7-S8**), indicating that the intermediate SiO_2 is essential.

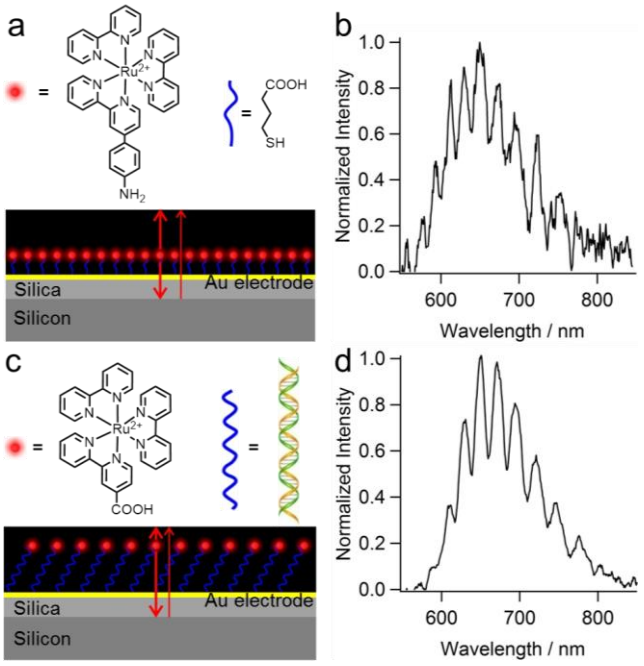

Figure 3. (a, c) Illustration of luminophore monolayers using MPA (a) and dsDNA (c) as the linker. (b, d) Normalized ECL self-interference spectra obtained for MPA- (b) and dsDNA-bridged (d) monolayers in phosphate buffer (PB) (0.2 M, pH 7.4) containing 30 mM DBAE. The potential was swept from 0.6 V to 1.2 V at a scan rate of 0.05 V/s.

According to matrix propagation model, ECL reflected by the film electrode can be also simplified to occur at a single front interface (**Figure S9**). Then ECL self-interference is equivalent to the interference of coherent light from two positions. The phase difference due to reflection at the front interface ($\Delta\varphi_R$) is given by (SI, Sections S2.2 and S3.2),

$$\Delta\varphi_R = \arctan\left[\frac{i n_0 (CB^* - BC^*)}{n_0^2 BB^* - CC^*}\right] \quad (3)$$

So the ECL self-interference spectrum can be calculated by (SI, Section S3.2 and **Figure S10**),

$$I(\lambda) = I_1(\lambda)[1 + R + 2\sqrt{R}\cos(\Delta\varphi)] \quad (4)$$

where $I_1(\lambda)$ is the intensity of ECL emitted directly by luminophores. Optimal matching with experimental ones (**Figure S11-S12**) gives us the extra path that the reflected beam travels. If only interference in the normal direction is monitored, the height of ECL luminophores at the electrode surface can be estimated as the half of extra path (**Figure S9**). The height of MPA- and dsDNA-bridged luminophores thus obtained was 1.5 nm and 8.7 nm, respectively. The former value is close to the distance between Ru and S atoms, namely 1.28 nm, estimated by ChemBio3D software. While the latter is smaller than that reported in literature (ca. 10.5 nm)[30], most likely due to the electrostatic attraction between negatively charged DNA strands and positively-biased electrode.[31] Furthermore, if assuming 50-bp dsDNA has a persistence length of

ca. 17 nm,[32] its tilt angle can be also calculated to be 59.2° (with respect to the normal). The results clearly prove that ECLIS has a high vertical nanoscale resolution. Indeed, fluorescence self-interference has been reported to possess even sub-nanometer vertical resolution.[33] We believe that ECLIS has additional advantages considering its near-zero background. Note that, although the spectrum (**Figure 3b**) was not that smooth due to relatively weak ECL emitted by the luminophore monolayer, the calculated height was still reliable because it was dominated by the position rather than intensity of peaks. This is indeed one of unique advantage of ECLIS.

We next employed ECLIS to probe the emitting layer adjacent to the electrode surface for ECL systems involving freely diffusing $Ru(bpy)_3^{2+}$ and TPrA, which is the most widely studied system. **Figure 4** displays self-interference spectra obtained at a low and high concentrations of $Ru(bpy)_3^{2+}$ (1 μM and 1 mM), which appear similar to those of luminophore monolayer (Normal ECL spectra with a single peak are always exhibited at the Au/glass electrode, **Figure S13**). Moreover, at 1 mM the spectral peaks show a bathochromic shift (side graph). Note that in solutions the emissive excited states ($Ru(bpy)_3^{2+*}$) are distributed in a thin layer near the electrode surface. If assuming (i) this layer can be divided into a number of sub-layers, (ii) each of them can be treated as a luminophore monolayer with a certain height and (iii) there exists a linear distribution profile of $Ru(bpy)_3^{2+*}$ (see details in SI, Section S4.2 and **Figure S14**), the overall spectrum can be calculated as the sum of those of all sub-layers. By optimal matching experimental and calculated spectra, the position of the highest sub-layer can be approximately considered as the thickness of emitting layer (TEL, **Figure S15**).

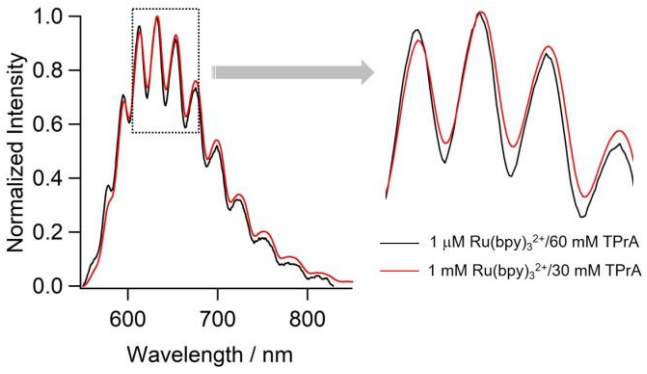

Figure 4. Normalized ECL self-interference spectra obtained with the $Au/SiO_2/Si$ electrode in PB (0.2 M, pH 7.4) containing 1 μM $Ru(bpy)_3^{2+}$/60 mM TPrA (black curve) and 1 mM $Ru(bpy)_3^{2+}$/30 mM TPrA (red curve). The applied potential was +1.2 V. The side graph shows the magnified view of four spectral peaks.

At a low concentration of $Ru(bpy)_3^{2+}$ (1 μM), the TEL was estimated to be ~350-450 nm. The TEL in this case is most likely determined by the surface concentration profile of $TPrA^{+\bullet}$ (**Figure S16**) that is known to extend over few micrometers. A much smaller TEL estimated here is likely due to the dramatic decrease of concentration of $TPrA^{+\bullet}$ within ~1 μm,[18] as well as the low concentration of $Ru(bpy)_3^{2+}$. ECL generation is confined to the surface and that far from the electrode surface is too low to be detected (**Figure S18**). While increasing the concentration of $Ru(bpy)_3^{2+}$, the value of TEL increased distinctly up to ~800-950 nm. As reported previously, under this condition the ECL generation is dominated by the "catalytic" route involving the homogenous oxidation of TPrA with $Ru(bpy)_3^{3+}$ (**Figure S17**).[17,34] Because the overall ECL reaction sequence is kinetically fast and $Ru(bpy)_3^{2+*}$ has a short diffusion distance (~20 nm),[17] we believe the TEL is determined by the diffusion of $Ru(bpy)_3^{3+}$. Therefore, a higher ECL intensity as well as thicker ECL emitting layer was obtained (**Figure S18**).

In summary, we present a novel yet simple optical interference technique based on ECL in-situ generated at the electrode surface, designated as ECLIS. With a high spatial resolution in the normal direction, it enables us to measure the height of ECL luminophores covalently immobilized on the electrode surface and the thickness of ECL emitting layer in solutions. The information is inaccessible by conventional ECL measurements but highly insightful for unraveling reaction mechanisms and developing immunoassays. We believe ECLIS will provide an easy way of studying interface chemistry processes.

ASSOCIATED CONTENT

Supporting Information. Experimental details; Matrix propagation model; Calculations of white light and ECL interference spectra; Additional ECL data (PDF). The Supporting Information is available free of charge on the ACS Publications website.

AUTHOR INFORMATION

Corresponding Author

*Prof. Bin Su, Email: subin@zju.edu.cn

Notes

The authors declare no competing financial interests.

ACKNOWLEDGMENTS

This work was supported by the Natural Science Foundation of China (21874117 and 21575126) and the Zhejiang Provincial Natural Science Foundation (LZ18B050001).

REFERENCES

(1) Richter, M. M. Electrochemiluminescence (ECL). *Chem. Rev.* **2004,** *104*, 3003-3036.

(2) Hu, L.; Xu, G. Applications and Trends in Electrochemiluminescence. *Chem. Soc. Rev.* **2010,** *39*, 3275-3304.

(3) Xu, L.; Li, Y.; Wu, S.; Liu, X.; Su, B. Imaging Latent Fingerprints by Electrochemiluminescence. *Angew. Chem., Int. Ed.* **2012,** *51*, 8068-8072.

(4) Xu, L.; Zhou, Z.; Zhang, C.; He, Y.; Su, B. Electrochemiluminescence Imaging of Latent Fingermarks through the Immunodetection of Secretions in Human Perspiration. *Chem. Commun.* **2014,** *50*, 9097-9100.

(5) Guo, W.; Ding, H.; Gu, C.; Liu, Y.; Jiang, X.; Su, B.; Shao, Y. Potential-Resolved Multicolor Electrochemiluminescence for Multiplex Immunoassay in a Single Sample. *J. Am. Chem. Soc.* **2018,** *140*, 15904-15915.

(6) Chen, L.; Hayne, D. J.; Doeven, E. H.; Agugiaro, J.; Wilson, D. J. D.; Henderson, L. C.; Connell, T. U.; Nai, Y. H.; Alexander, R.; Carrara, S.; Hogan, C. F.; Donnelly, P. S.; Francis, P. S. A Conceptual Framework for the Development of Iridium(III) Complex-Based Electrogenerated Chemiluminescence Labels. *Chem. Sci.* **2019,** *10*, 8654-8667.

(7) Valenti, G.; Scarabino, S.; Goudeau, B.; Lesch, A.; Jović, M.; Villani, E.; Sentic, M.; Rapino, S.; Arbault, S.; Paolucci, F.; Sojic, N. Single Cell Electrochemiluminescence Imaging: From the Proof-of-Concept to Disposable Device-Based Analysis. *J. Am. Chem. Soc.* **2017,** *139*, 16830-16837.

(8) Voci, S.; Goudeau, B.; Valenti, G.; Lesch, A.; Jović, M.; Rapino, S.; Paolucci, F.; Arbault, S.; Sojic, N. Surface-Confined Electrochemiluminescence Microscopy of Cell Membranes. *J. Am. Chem. Soc.* **2018,** *140*, 14753-14760.

(9) Zhang, J.; Jin, R.; Jiang, D.; Chen, H.-Y. Electrochemiluminescence-Based Capacitance Microscopy for Label-Free Imaging of Antigens on the Cellular Plasma Membrane. *J. Am. Chem. Soc.* **2019,** *141*, 10294-10299.

(10) Chang, Y. L.; Palacios, R. E.; Fan, F. R. F.; Bard, A. J.; Barbara, P. F. Electrogenerated Chemiluminescence of Single Conjugated Polymer Nanoparticles. *J. Am. Chem. Soc.* **2008,** *130*, 8906-8907.
(11) Hesari, M.; Ding, Z. A Grand Avenue to Au Nanocluster Electrochemiluminescence. *Acc. Chem. Res.* **2017,** *50*, 218-230.
(12) Ma, C.; Wu, W.; Li, L.; Wu, S.; Zhang, J.; Chen, Z.; Zhu, J.-J. Dynamically Imaging Collision Electrochemistry of Single Electrochemiluminescence Nano-Emitters. *Chem. Sci.* **2018,** *9*, 6167-6175.
(13) Zhu, M. J.; Pan, J. B.; Wu, Z. Q.; Gao, X. Y.; Zhao, W.; Xia, X. H.; Xu, J. J.; Chen, H. Y. Electrogenerated Chemiluminescence Imaging of Electrocatalysis at a Single Au - Pt Janus Nanoparticle. *Angew. Chem. Int. Ed.* **2018,** *130*, 4074-4078.
(14) Guo, W.; Liu, Y.; Cao, Z.; Su, B. Imaging Analysis Based on Electrogenerated Chemiluminescence. *J. Anal. Test.* **2017,** *1*, 1-14.
(15) Wang, Y.; Cao, Z.; Yang, Q.; Guo, W.; Su, B. Optical Methods for Studying Local Electrochemical Reactions with Spatial Resolution: A Critical Review. *Anal. Chim. Acta* **2019,** *1074*, 1-15.
(16) Collinson, M. M.; Pastore, P.; Maness, K. M.; Wightman, R. M. Electrochemiluminescence Interferometry at Microelectrode. *J. Am. Chem. Soc.* **1994,** *116*, 4095-4096.
(17) Chovin, A.; Garrigue, P.; Vinatier, P.; Sojic, N. Development of an Ordered Array of Optoelectrochemical Individually Readable Sensors with Submicrometer Dimensions: Application to Remote Electrochemiluminescence Imaging. *Anal. Chem.* **2004,** *76*, 357-364.
(18) Miao, W.; Choi, J.-P.; Bard, A. J. Electrogenerated Chemiluminescence 69: The Tris(2,2'-bipyridine)ruthenium(II), $(Ru(bpy)_3^{2+})$/Tri-*n*-propylamine (TPrA) System Revisited-A New Route Involving $TPrA^{\bullet+}$ Cation Radicals. *J. Am. Chem. Soc.* **2002,** *124*, 14478-14485.
(19) Macleod, H. A. *Thin-Film Optical Filters*. CRC press: 2010.
(20) Bornhop, D. J.; Latham, J. C.; Kussrow, A.; Markov, D. A.; Jones, R. D.; Sorensen, H. S. Free-Solution, Label-Free Molecular Interactions Studied by Back-Scattering Interferometry. *Science* **2007,** *317*, 1732-1736.
(21) Orosco, M. M.; Pacholski, C.; Sailor, M. J. Real-Time Monitoring of Enzyme Activity in a Mesoporous Silicon Double Layer. *Nat. Nanotechnol.* **2009,** *4*, 255-258.
(22) Law, C. S.; Sylvia, G. M.; Nemati, M.; Yu, J.; Losic, D.; Abell, A. D.; Santos, A. Engineering of Surface Chemistry for Enhanced Sensitivity in Nanoporous Interferometric Sensing Platforms. *ACS Appl. Mater. Interfaces* **2017,** *9*, 8929-8940.
(23) Smith, C. P.; Kennedy, H. L.; Kragt, H. J.; White, H. S.; Biegen, J. F. Phase-Measurement Interferometric Microscopy of Microlithographically Fabricated Platinum Electrodes. *Anal. Chem.* **1990,** *62*, 1135-1138.
(24) Singh, G.; Moore, D.; Saraf, R. F. Localized Electrochemistry on a 10 µm Spot on a Monolith Large Electrode: An Avenue for Electrochemical Microarray Analysis. *Anal. Chem.* **2009,** *81*, 6055-6060.
(25) Roy, S.; Prasad, A.; Tevatia, R.; Saraf, R. F. Heavy Metal Ion Detection on a Microspot Electrode Using an Optical Electrochemical Probe. *Electrochem. Commun.* **2018,** *86*, 94-98.
(26) Tevatia, R.; Prasad, A.; Saraf, R. F. Electrochemical Characteristics of a DNA Modified Electrode as a Function of Percent Binding. *Anal. Chem.* **2019,** *91*, 10501-10508.
(27) Alvarez, S. D.; Li, C.-P.; Chiang, C. E.; Schuller, I. K.; Sailor, M. J. A Label-Free Porous Alumina Interferometric Immunosensor. *ACS Nano* **2009,** *3*, 3301-3307.
(28) Baksh, M. M.; Kussrow, A. K.; Mileni, M.; Finn, M. G.; Bornhop, D. J. Label-Free Quantification of Membrane-Ligand Interactions Using Backscattering Interferometry. *Nat. Biotechnol.* **2011,** *29*, 357-360.
(29) Kussrow, A.; Enders, C. S.; Bornhop, D. J. Interferometric Methods for Label-Free Molecular Interaction Studies. *Anal. Chem.* **2012,** *84*, 779-792.
(30) Moiseev, L.; Unlu, M. S.; Swan, A. K.; Goldberg, B. B.; Cantor, C. R. DNA Conformation on Surfaces Measured by Fluorescence Self-Interference. *Proc. Natl. Acad. Sci. U. S. A.* **2006,** *103*, 2623-2628.
(31) Kaiser, W.; Rant, U. Conformations of End-Tethered DNA Molecules on Gold Surfaces: Influences of Applied Electric Potential, Electrolyte Screening, and Temperature. *J. Am. Chem. Soc.* **2010,** *132*, 7935-7945.
(32) Spuhler, P. S.; Sola, L.; Zhang, X.; Monroe, M. R.; Greenspun, J. T.; Chiari, M.; Unlu, M. S. Precisely Controlled Smart Polymer Scaffold for Nanoscale Manipulation of Biomolecules. *Anal. Chem.* **2012,** *84*, 10593-10599.
(33) Swan, A. K.; Moiseev, L. A.; Cantor, C.; Davis, B.; Ippolito, S.; Karl, W. C.; Goldberg, B. B.; Unlu, M. Toward Nanometer-Scale Resolution in Fluorescence Microscopy Using Spectral Self-Interference. *IEEE J. Sel. Top. Quantum Electron.* **2003,** *9*, 294-300.
(34) Zu, Y.; Bard, A. J. Electrogenerated Chemiluminescence. 66. The Role of Direct Coreactant Oxidation in the Ruthenium Tris(2,2')bipyridyl/Tripropylamine System and the Effect of Halide Ions on the Emission Intensity. *Anal. Chem.* **2000,** *72*, 3223-3232.

For Table of Contents Only